Journal of The Electrochemical Society, **162** (6) A1055-A1066 (2015)
0013-4651/2015/162(6)/A1055/12/$33.00 © The Electrochemical Society

A Study of the Influence of Lithium Salt Anions on Oxygen Reduction Reactions in Li-Air Batteries

Iromie Gunasekara,[a,*] Sanjeev Mukerjee,[a,] Edward J. Plichta,[b] Mary A. Hendrickson,[b] and K. M. Abraham[a,**,z]**

[a]*Department of Chemistry and Chemical Biology, Northeastern University, Boston, Massachusetts 02115, USA*
[b]*Power Division, US Army RDECOM CERDEC CP&I, RDER-CCP, Aberdeen Proving Ground, Maryland 21005, USA*

The influence of lithium salts on O_2 reduction reactions (ORR) in 1, 2-dimethoxyethane (DME) and tetraethylene glycol dimethyl ether (TEGDME) has been investigated. Microelectrode studies in a series of tetrabutylammonium salt (TBA salt)/DME-based electrolytes showed that O_2 solubility and diffusion coefficient are not significantly affected by the electrolyte anion. The ORR voltammograms on microelectrodes in these electrolytes exhibited steady-state limiting current behavior. In contrast, peak-shaped voltammograms were observed in Li^+-conducting electrolytes suggesting a reduction of the effective electrode area by passivating ORR products as well as migration-diffusion control of the reactants at the microelectrode. FT-IR spectra have revealed that Li^+ ions are solvated to form solvent separated ion pairs of the type $Li^+(DME)_nPF_6^-$ and $Li^+(TEGDME)PF_6^-$ in $LiPF_6$-based electrolytes. On the other hand, the contact ion pairs $(DME)_mLi^+(CF_3SO_3^-)$ and$(TEGDME)Li^+(CF_3SO_3^-)$ appear to form in $LiSO_3CF_3$-containing electrolytes. In the $LiSO_3CF_3$–based electrolytes the initial ORR product, superoxide (O_2^-), is stabilized in solution by forming $[(DME)_{m-1}(O_2^-)]Li^+(CF_3SO_3^-)$ and $[(TEGDME)(O_2^-)]Li^+(CF_3SO_3^-)$ complexes. These soluble superoxide complexes are able to diffuse away from the electrode surface reaction sites to the bulk electrolyte in the electrode pores where they decompose to form Li_2O_2. This explains the higher capacity obtained in Li/O_2 cells utilizing $LiCF_3SO_3$/TEGDME electrolytes.
 [DOI: 10.1149/2.0841506jes]

Manuscript submitted January 26, 2015; revised manuscript received March 3, 2015. Published March 19, 2015.

The Li-air battery with a theoretical energy density many times higher than that of Li-ion batteries,[1] has gained world-wide attention as a potential energy source for the development of long range electrical vehicles as well as many other energy hungry applications in the defense and civilian sectors. The promise of the high theoretical energy density has not yet been translated into practical devices due to the shortcomings of the electrode and electrolyte materials used in the battery as well as an incomplete understanding of the chemical and electrochemical processes involved in its operation. In our previous publications we have shown the strong effect of non-aqueous solvents on the oxygen reduction reaction (ORR) electrochemistry in Li^+-containing electrolytes.[2–7] We have also successfully employed a carbon microelectrode to quantify oxygen transport parameters and elucidate the influence of the Li salt on the reversibility of the ORR in tetrabutylammonium and lithium salt-containing electrolytes in dimethyl sulfoxide (DMSO).[8,9] It has become increasingly clear that the ORR in the non-aqueous Li-air battery is highly solvent controlled[10] with a secondary role of the Li salt through the solvates formed between the solvent and the salt.[11]

The stability of the electrolyte solvent in contact with the O_2 reduction products in the non-aqueous Li-air battery plays a key role on the reversibility of the oxygen reduction reactions (ORR). Organic carbonate solvents such as propylene carbonate (PC), ethylene carbonate (EC) and diethyl carbonate (DEC) readily decompose through their reactions with the superoxide (O_2^-) radicals formed as the ORR intermediate in these electrolyte media.[12–14] Ethers are recognized as relatively stable solvents without significant superoxide mediated decomposition.[15] Ethers are also important due to their high oxygen solubility and low to moderate dielectric constants resulting in lower reactivity towards the superoxide ions. In this paper, we present ORR electrochemistry data gathered from electrolytes in, 1, 2-dimethoxyethane (DME) and tetraethylene glycol dimethyl ether (TEGDME), ethers that have been studied as solvents for Li-air batteries. Their low dielectric constants (DME, 7.07 and TEGDME, 7.79)[16,17] are important as this property influences the wettability of the carbon cathode and provide better stability in the presence of ORR products. Even though DME is a low boiling point solvent, its ability to form well conductive electrolytes makes it an attractive representative medium to elucidate ORR mechanism in ether-based electrolytes. TEGDME is especially desirable as a practical solvent for Li-air batteries because of its low vapor pressure and other desirable properties as we stated in our original reason for the selection of this solvent.[6,7,18]

In our previous publication on the utility of microelectrodes for Li-air battery diagnostics, we presented a detailed analysis of the ORR in an electrolyte based on a high Donor Number (Lewis basicity) solvent namely, DMSO (DN = 29 kcal/mole).[8] TEGDME and DME on the other hand, are low Donor Number solvents (DN = 16.6 and 20 kcal/mole, respectively). It is our expectation that with the microelectrode studies presented in this paper together with the previous work in DMSO, we would provide a fuller picture of the extent to which the electron donor properties of the solvent and Li salt anion, as well as the transport of O_2 in the electrolyte, influence the mechanism and reversibility of the ORR in non-aqueous Li-air batteries. FT-IR spectral data provided information on the structures of the electrolyte solutions to enable us to correlate O_2 electrochemistry with electrolyte properties.

Experimental

Materials.— All tetrabutylammonium (TBA) salts ($TBAPF_6$, $TBACF_3SO_3$, $TBAN(CF_3SO_2)_2$, $TBAClO_4$) and lithium salts ($LiPF_6$, $LiCF_3SO_3$, $LiN(CF_3SO_2)_2$, $LiClO_4$), battery grade, were purchased from Sigma-Aldrich and were stored in an MBraun glove-box maintained under 0.5 ppm humidity. An 11 μm diameter carbon disk microelectrode working electrode purchased from BASi and a Pt mesh counter electrode were used. A $Ag/AgNO_3$ reference electrode was prepared as reported by Wain et al.[19] using silver wire (99%) purchased from Alfa Aesar. All the potentials in this paper are reported with respect to the Li/Li^+ scale obtained using a conversion factor determined by measuring the potential of Ag/Ag^+ reference electrode versus a Li foil reference electrode in each electrolyte.

Cyclic voltammetry.— Cyclic voltammograms were recorded in argon saturated solutions to verify that the electrolyte itself does not undergo any reaction within the electrochemical potential window of interest. All the current densities reported in this paper are referenced to the geometric surface areas of the electrodes. Oxygen electrochemistry was recorded at the carbon microelectrode (5.5 μm electrode radius) in O_2 saturated DME and TEGDME-based electrolytes. Current-time transients were obtained in TBA/DME salt electrolytes, by stepping the microelectrode potential from a potential where there is no reaction to a potential where the reaction is diffusion limited. Oxygen transport parameters were calculated using Cottrell

*Electrochemical Society Student Member.
**Electrochemical Society Fellow.
zE-mail: kmabraham@comcast.net

plots obtained from these potential jump experiments. Oxygen reduction electrochemistry was also performed in a series of Li salt-based electrolytes ($LiPF_6$, $LiCF_3SO_3$, $LiN(CF_3SO_2)_2$ and $LiClO_4$) in DME and in TEGDME.

Most of the cyclic voltammograms at the carbon microelectrode were recorded at a scan rate of 200 mVs^{-1}. This is a relatively high scan rate. However, charging currents are minimal at a microelectrode and this allows us to record cyclic voltammograms at high scan rates at these electrodes without sacrificing any electrochemical information. In fact, a high 200 mVs^{-1} scan rate is preferred for studying electrochemical processes in Li^+-based electrolytes in order to avoid rapid passivation of the microelectrode surface by insoluble lithium oxide products.

RRDE measurements.— Electrochemical measurements were also obtained at a rotating ring disk electrode (RRDE) in Li salt/TEGDME electrolytes. The rotating ring disk consisted of a glassy carbon working electrode and a gold ring secondary working electrode. The gold ring was set at a positive potential where the oxidation of the lithium oxides produced from the reduction of O_2 on the carbon disk occurred.

Ring efficiency.—Ring efficiency of the rotating ring disk electrode was determined as follows. Ferrocene was oxidized in an argon-purged Li salt/TEGDME solution where the ring potential was set to a potential where the reduction of ferrocenium ion produced from the oxidation reaction occurred. Ring efficiency was calculated from the ratio of the ring current to the disk current.

All electrochemical tests were carried out in a glove-box maintained at a humidity level < 0.5 ppm.

Lithium-air cell testing.— Lithium-air full cells were constructed as previously reported[3] using Li foil anodes and KetjenBlack (EC300JD) or Vulcan XC-72R carbon porous cathodes, and microporous polypropylene membrane separators. Discharged cathodes were analyzed by means of a Rigaku X-ray diffractometer with the samples sealed in Kapton polyimide film to identify the discharge products.

FT-IR characterization.— A series of electrolytes composed of Li salt solution in DME or TEGDME were analyzed using a Bruker Vertex-70 FT-IR spectrometer.

Results and Discussion

Preliminary electrochemical data gathered in TBA salt/DME-based electrolytes at a rotating disk electrode (RDE) showed that the ORR does not reach a limiting current within the stable potential window of the electrolyte. This is because oxygen reduction reaction is kinetically, not mass transport, limited in DME-based electrolytes. Therefore, it is impossible to calculate the oxygen transport parameters with the aid of the RDE technique in these electrolytes. However, efficient oxygen transport observed at a microelectrode can be useful to obtain steady-state limiting current conditions. From these steady-state current-potential data at the microelectrode, one can calculate oxygen transport parameters in these electrolytes which are useful for the development of practical Li-air batteries.[20,21] The first part of this paper details our microelectrode studies in DME-based electrolytes. In the second part we extend the studies to electrolytes in the high molecular weight ether, TEGDME. The TEGDME is a low volatile solvent with a donor number of 16.6 kcal/mole, which following our original investigation[2,18,22] has been studied as a Li-air battery electrolyte, by many researchers.[6,7,22–24] As we reported previously, the electron donor property of a solvent influences the mechanism and reversibility of the ORR in lithium salt-containing electrolytes through the Hard Soft Acid Base concept.[2,4] The quantitative effect of the Donor Number of the solvent on ORR can only be investigated in the absence of Li ions which otherwise would complicate the analysis by passivating the electrode surface with ORR products. However, oxygen transport properties and electrochemistry in tetrabutylammonium salt (TBA salt)-containing TEGDME electrolytes, in which passivation of the electrode surface does not occur, has not been satisfactorily performed using planar glassy carbon macro disk electrodes due to the high viscosity and the associated large *iR* drop and kinetic limitations of the ORR in the stable potential window of these electrolytes. Electrochemistry on a microelectrode is able to overcome these limitations by allowing us to study diffusion limited ORR in these electrolytes to determine oxygen transport properties, as well as ORR kinetics and mechanisms.

Microelectrode electrochemistry.— A microelectrode has the unique advantage of efficient transport of electro-active species to and from the electrode surface. This is demonstrated by the sigmoidal-shaped cyclic voltammograms that we have observed[8] in ferrocene solution in DMSO at scan rates as high as 500 mV s^{-1}. The diffusion controlled limiting current at a micro-disk electrode is given by equation 1.

$$I_d = \frac{4nFADC}{\pi r} = 4nFDCr \qquad [1]$$

In equation 1, I_d is the diffusion limited current, F is the Faraday constant, A is the geometric area of the electrode, n is the number of electrons, r is the electrode radius and D and C are diffusion coefficient and solubility of the electroactive species, respectively.

We have also shown that the oxygen transport to a 5.5 μm radius microelectrode in DMSO[8] is approximately equal to the hydrodynamic transport of oxygen to a rotating disk electrode at a speed of 25000 rpm. Ohmic drops originating from solution resistance are minimal on microelectrodes due to the very small current values involved. Other advantages and theoretical considerations of ORR on microelectrodes in non-aqueous electrolytes have been presented in our previous paper.[8]

Oxygen transport and ORR in tetrabutylammonium salt based ether electrolytes: - the effect of the electrolyte salt anion.

1,2-Dimethoxyethane (DME).— Dimethoxyethane has been widely used as a solvent in Li batteries, and particularly as a co-solvent with carbonate-based electrolytes. There are several studies discussing O_2 electrochemistry in PC: DME mixed solvent electrolytes.[12,15,25,26] The reasons for adding DME as a co-solvent to PC-based electrolytes are several; its low reactivity towards lithium, a low viscosity of 0.402 centipoise (cP)[27] which lowers the overall viscosity of the PC: DME mixed electrolytes, and the relatively large potential stability window. The current versus potential scans for O_2 on the microelectrode in $TBACF_3SO_3$/DME electrolyte, shown in Figure 1A, depict a sigmoidal shaped voltammogram with a limiting current independent of the scan rate. The data are consistent with a one- electron reversible reaction (equation 2) with no passivation film formation at the electrode surface.[8]

$$O_2 + e^- \leftrightharpoons O_2^- \qquad [2]$$

Figure 1B depicts steady state voltamograms obtained on the carbon microelectrode in a series of TBA salt solutions in DME. These steady-state voltammograms obtained in 0.1 M solutions of $TBAPF_6$, $TBACF_3SO_3$, $TBAN(CF_3SO_2)_2$ and $TBAClO_4$ in DME at 200 mV s^{-1} all show similar limiting currents, suggesting the same magnitude of oxygen transport rate (permeability values) in all of the electrolytes.

When the microelectrode is stepped from a potential where there is no reaction to a potential where the reaction is diffusion limited, the current (I in Ampere)-time (t in seconds.) transient at small times after polarization can be related by equation 3.

$$I = \frac{nFAD^{\frac{1}{2}}C}{\pi^{\frac{1}{2}}t^{\frac{1}{2}}} + n\pi FDCr \qquad [3]$$

Current-time transients were obtained by holding the electrode potential at 2.6 V for 100 sec and then stepping the electrode potential to 1.2 V. Cottrell plots calculated from these current-time transients in each electrolyte are shown in Figure 1C. The oxygen diffusion coefficients and oxygen solubility values we have calculated from these

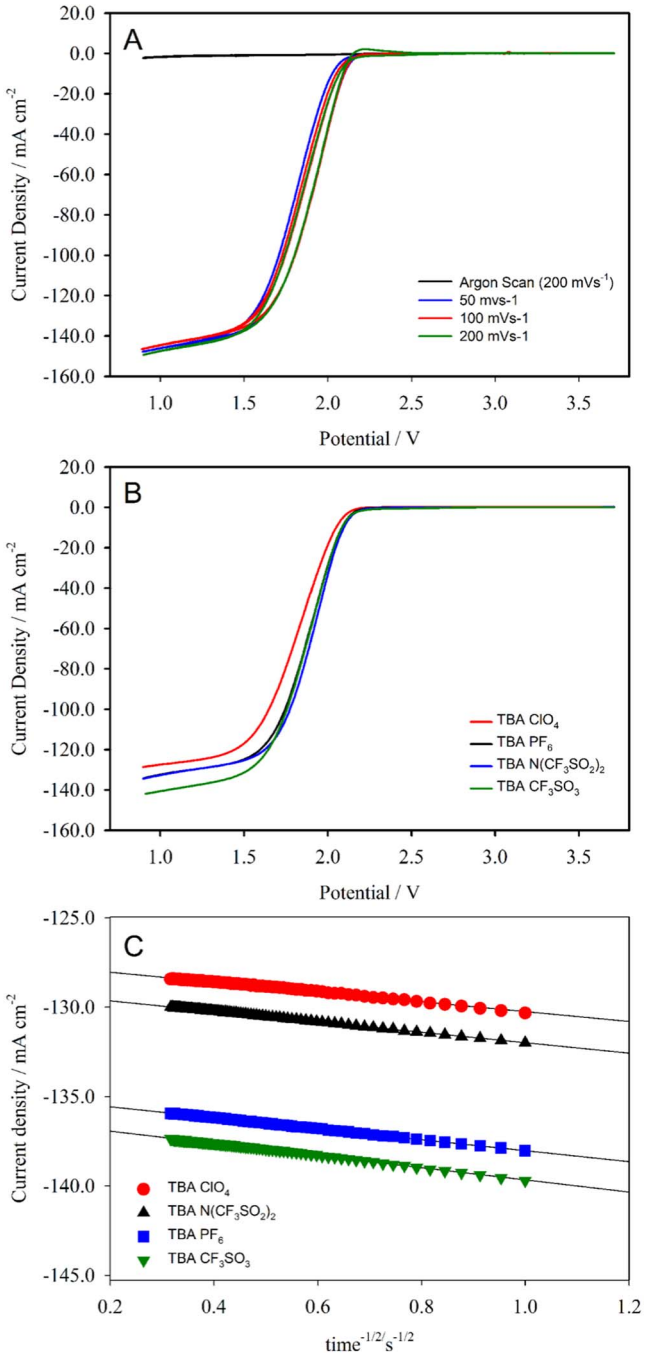

Figure 1. Oxygen reduction limiting currents obtained on the carbon microelectrode A) in 0.1 M $TBACF_3SO_3$/DME at several voltage scan rates from 50–200 mVs^{-1} (CV recorded at 200 mVs^{-1} in an Ar saturated electrolyte is shown in black), B) in a series of 0.1 M TBA salt/DME electrolytes at 200 mV s^{-1}. C) Cottrell plots obtained for the current time transients recorded in an O_2 saturated series of TBA salt/DME electrolytes.

data are listed in Table I. The similar oxygen diffusion and solubility values obtained in all electrolytes reveal that the anion of the salt has a negligible effect on the oxygen transport in the DME electrolytes. The oxygen diffusion coefficient calculated here for $LiPF_6$/DME solution is higher than the value we previously determined from Tafel data.[2] However, the values reported here are probably more accurate since this determination does not involve the effects of Ohmic drop and electrode roughness encountered in Tafel calculations. The present data reveals that DME has a very high oxygen transport which is keeping with its low viscosity. Furthermore, we believe that the low polarity

Table I. Oxygen transport parameters in 1,2-dimethoxyethane.

TBA salt (0.1 M in DME)	O_2 Diffusion Coefficient/10^{-4} cm^2 s^{-1}	O_2 Solubility/mM
$TBAPF_6$	1.79	4.28
$TBAClO_4$	1.82	3.91
$TBACF_3SO_3$	1.58	5.08
$TBAN(CF_3SO_2)_2$	1.75	4.14

of DME which would decrease dipolar interactions between DME and O_2 also would lead to higher oxygen diffusion coefficient in this solvent.[8] Oxygen transport parameters directly impact the discharge capacity and the rate of O_2 cathode reaction in the Li-O_2 battery. This finding not only reiterates the role of DME as a good solvent to study ORR but also promotes the view that ethers are suitable solvents in terms of mass transport for Li-O_2 batteries.[28]

Tetraethylene glycol dimethyl ether (TEGDME).—The high molar weight $TBAPF_6$ is sparingly soluble in the viscous TEGDME. Initially, a $TBAPF_6$ saturated solution of TEGDME with an approximate salt concentration of less than 0.1 M was used as the electrolyte. Steady-state ORR currents were observed only at very low potentials (Figure 2A). As we stated in our previous publication,[8] the steady-state behavior observed in this TBA electrolyte indicates that the ORR terminates at the one-electron reduction product superoxide (with no further reduction to peroxides). These data also affirm reversible O_2 electrochemistry with little passivation of the electrode surface in this electrolyte.

For further analysis, ORR in 0.1 M solution of $TBACF_3SO_3$ in TEGDME was investigated. $TBACF_3SO_3$ was more soluble in TEGDME. Again, limiting current independent of the scan rates confirmed one-electron reduction of oxygen to superoxide ion in $TBACF_3SO_3$/TEGDME. The low charge density (weak acid) of TBA^+ enhances the stability of the weak base superoxide ion in the electrolyte by forming the ion pair TBA^+–O_2^-, in conformity with the Hard Soft Acid Base (HSAB) concept. This observation is reminiscent of our findings in TBA salt-based electrolytes in DMSO and the results observed in DME.[2,23] As the potential scan rate was decreased to 5 mV s^{-1}, a suppression of the steady-state current was observed with practically no current at 1.5 mV s^{-1} (Figure 2C). A possible reason for the diminishing currents at very low scan rates is that the initially formed superoxide ions have some reaction with TEGDME to form passivating products on the electrode and block the electrode surface to varying levels depending on the scan rate. We can also conclude from the sigmoidal-shaped voltammogram at 5 mV s^{-1} that there is no further electrochemical reduction of the superoxide ions in $TBACF_3SO_3$/TEGDME electrolyte at these potentials.

Oxygen diffusion rate and solubility in $TBACF_3SO_3$/TEGDME were calculated using the Cottrell plot (equation 3, Figure 2D) obtained from chronoamperometric current-time transients.[8,21] Oxygen solubility was found to be 3.5 mM and the oxygen diffusion coefficient was calculated to be 3.5×10^{-5} cm^2 s^{-1}. The oxygen solubility value is in agreement with that we previously reported for $LiPF_6$/TEGDME electrolyte.[2] The oxygen diffusivity determined in this work is considerably higher than what was previously reported in 0.1 M $LiPF_6$/TEGDME.[2] However, the theoretical ORR limiting current calculated from equation 1 using the diffusivity and solubility values determined in this study is in agreement with the observed ORR limiting current in this electrolyte. Therefore, we conclude that the oxygen diffusivity in $TBACF_3SO_3$/TEGDME electrolyte is higher than the previously determined value in $LiPF_6$/TEGDME.

Although the actual Li salt concentration in the electrolytes used in Li-O_2 batteries is much higher than the 0.1M TBA salt solutions we used in the O_2 transport measurements, we believe that the transport data from the dilute TBA salt solutions can be used to project O_2 transport in the 1M solutions in the Li-air battery. This is because, the motion of the neutral O_2 molecule in the electrolyte is minimally affected by the ionic environment.

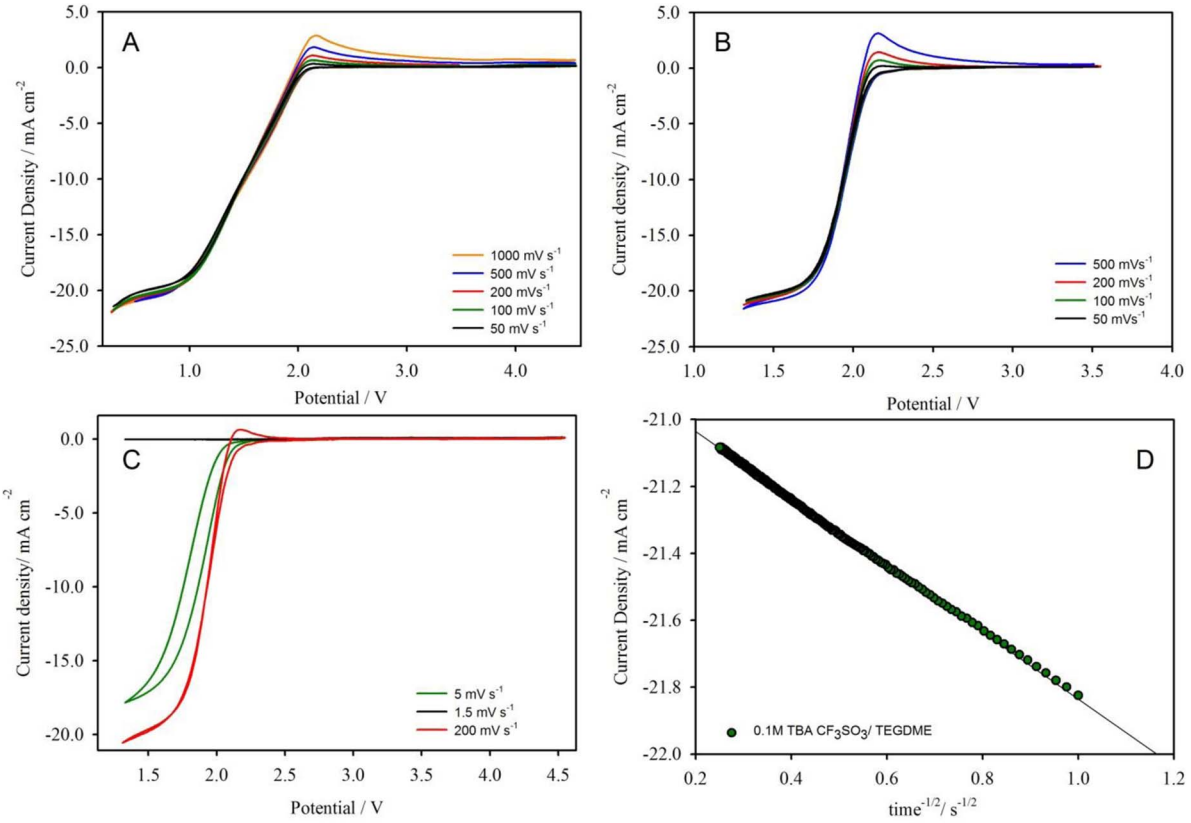

Figure 2. Oxygen reduction limiting currents obtained on the carbon microelectrode in a A) saturated TBA PF_6/TEGDME, B-C) 0.1 M TBA CF_3SO_3/TEGDME electrolyte. D) Cottrell plot obtained for the current time transient obtained in O_2 saturated 0.1 M TBA CF_3SO_3/TEGDME electrolyte.

ORR in Li salt solutions in 1,2-Dimethoxyethane (DME) and tetraethylene glycol dimethyl ether (TEGDME).

Li salt solutions in DME–based electrolytes.— Microelectrode voltammograms for ORR in Li salt/DME solutions showed peak-shaped behavior. As we discussed before[8] microelectrode response can deviate from the expected steady-state behavior observed for O_2 in $TBAPF_6$/DME (Figure 1A), due to two main reasons: i) the electrostatic repulsion of the species being reduced at the commencement of the second reduction reaction of the initial ORR product, i.e, reduction of O_2^- to O_2^{2-} (equation 4)

$$O_2^- + e^- \rightarrow O_2^{2-} \qquad [4]$$

and ii) from passivation of the electrode surface by the ORR product(s), e.g; Li_2O_2. Bell shaped oxygen reduction currents in Li salt/DME solutions (Figure 3A (blue) and Figure 3B) suggest that further electrochemical reduction of the initially formed superoxide ion (O_2^-) to peroxide (O_2^{2-}) occurs at lower potentials[8] along with electrode passivation by the deposition of this product on the electrode surface. As a test of the cyclability of the ORR/OER processes, we repeated the CV in 0.1 M $LiPF_6$/DME at 200 mV s^{-1} (Figure 3B – red (200 mV s^{-1}) and it showed zero reduction current in the second cycle (Figure 3B – black dotted line), which was surprising considering the very low columbic efficiency (zero anodic current) in the first cycle. The latter behavior on a microelectrode is usually indicative of solubility of the ORR products.[8] Figure 3A reveals a significantly smaller peak current in $LiPF_6$/DME than the steady state current seen in $TBAPF_6$/DME. This contrasts with our previous obervation in DMSO-based electrolytes in which, ORR in TBA and Li salt-containing solutions showed similar limiting or peak currents.

The ORR/OER behavior in $LiCF_3SO_3$/DME was markedly different from that in the $LiPF_6$ solution. In the $LiCF_3SO_3$ electrolyte similar ORR currents were seen in the 1st and the 12th cycles as depicted in Figure 4B. These opposing ORR behavior in presence of the two electrolytes certainly need an explanation. In order to ascertain if the current reduction with cycling in $LiPF_6$/DME is caused by the passivation of the electrode surface, we have used a technique that we previously developed. This involves determining whether there is any suppression of ORR limiting currents on the microelectrode in a $TBAPF_6$/ DMSO-based electrolyte after the ORR in $LiPF_6$/DME on the same electrode. The ORR limiting current recorded in 0.1M $TBAPF_6$/ DMSO after one ORR half cycle in $LiPF_6$/DME is shown in Figure 5.

The result reveals that the electrode has become completely passivated in $LiPF_6$/DME after the ORR without any ability for it to sustain O_2 reduction in $TBAPF_6$/ DMSO solution. In addition, the fact that the Columbic efficiency of the reaction in $LiPF_6$/DME did not improve by limiting the cathodic potential to 2.0 V suggests that the electrode passivation occurs from the beginning of ORR at higher potentials, most probably by the chemical decomposition of the initially formed lithium superoxide to insoluble Li_2O_2 (Figure 3C) as depicted in equation 5.

$$2LiO_2 \rightarrow Li_2O_2 + O_2 \qquad [5]$$

The high degree of passivation in $LiPF_6$-based electrolyte suggests that the peak shape of the CV is the result of electrode passivation in addition to migration- diffusion control of the first reduction product.

The information which can be obtained from the voltammograms recorded in $LiPF_6$/DME is limited due to the instant passivation of the electrode surface during the first half-cycle of the ORR. Therefore, further analysis of the DME- based electrolyte system was carried out in 0.1M $LiCF_3SO_3$/DME. Figure 4A shows oxygen reduction reaction electrochemistry recorded in this electrolyte for different cathodic limits at the sweep rate of 200 mV s^{-1}. A small shoulder peak appeared around 2.2 V in the reduction scan (Figure 4C). However, when the cathodic scan was limited to 2.12 V, there was no significant

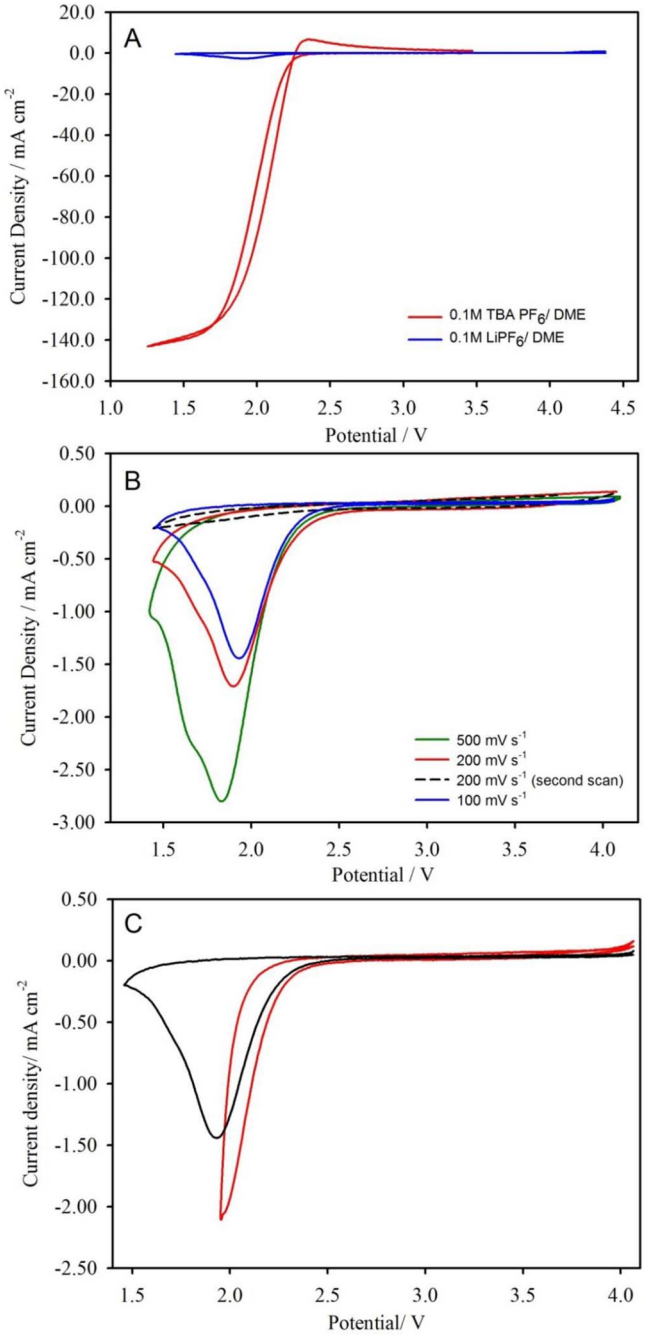

Figure 3. A) Current-voltage data obtained on the carbon microelectrode in 0.1 M $TBAPF_6$/DME (red), and 0.1 M $LiPF_6$/DME (blue). B) Scan rate dependent cyclic voltammograms obtained on the carbon microelectrode in 0.1M $LiPF_6$/DME (continuously recorded second CV at 200 mVs^{-1} is shown as a black dotted line, C) Comparison of anodic current-potential response on the microelectrode with different cathodic potential limits at 200 mV s^{-1}.

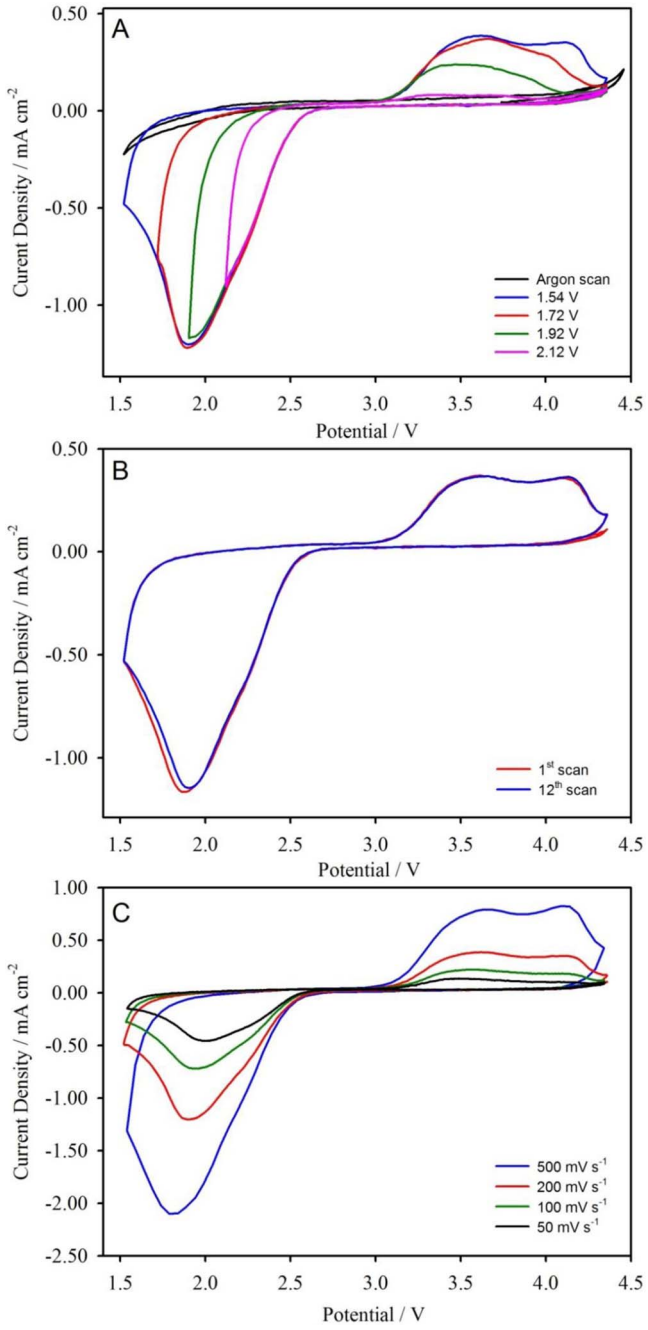

Figure 4. Cyclic voltammograms recorded at the 11 μm carbon electrode in O_2 saturated electrolytes. A) anodic response in $LiCF_3SO_3$/DME at different cathodic limiting potentials. B) Cyclability of the ORR/OER in $LiCF_3SO_3$/DME, C) Scan rate dependent ORR/OER in $LiCF_3SO_3$/DME.

response observed in the anodic scan. This, along with the improved cyclability of the ORR/OER processes in this electrolyte implies that the reduction shoulder peak which appears around 2.2 V is probably from the initial one-electron reduction of the O_2 to superoxide. It should be noted that the current peak in $LiCF_3SO_3$/DME appears at slightly lower potentials than in $LiPF_6$/DME.

Oxygen electrochemistry in $LiPF_6$ and $LiCF_3SO_3$ solutions in TEGDME.—The voltammograms for oxygen reduction reactions at a carbon microelectrode in $LiPF_6$/TEGDME are shown in Figure 6A. We observed bell shaped oxygen reduction curves for a range of scan rates, which as described above can be explained on the basis of the migration-diffusion controlled currents originating from the initial one-electron O_2 reduction product LiO_2, and its one-electron reduction to Li_2O_2.[8,24]

Cyclic voltamograms recorded at different cathodic limiting potentials provided interesting insights. First, an anodic peak appeared when the potential was scanned cathodically down to 2.15 V, which grew when the cathodic limit was decreased. This is attributed to the formation and re-oxidation of Li_2O_2. When the cathodic potential was limited to 1.7 V, another anodic peak emerged which is attributed to the oxidation of the ORR product Li_2O.

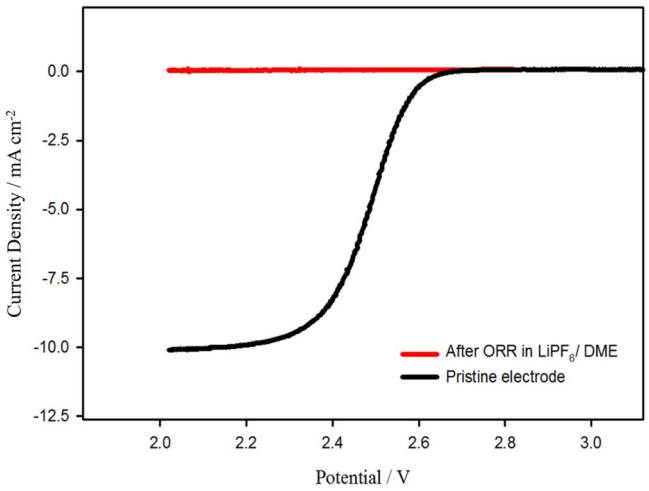

Figure 5. Oxygen reduction half-cycles were recorded at a pristine carbon microelectrode in $LiPF_6$/DME. ORR limiting currents recorded for the same electrode in $TBAPF_6$/DMSO soon after the above reaction are shown.

Continuous scanning of potentials between 1.5 V and 4.5 V in $LiPF_6$/TEGDME electrolyte showed rapid decaying of the ORR peak current density (Figure 7A). This observation conforms with the above conclusion that Li_2O is formed at low potentials. The oxidation overpotential of crystalline lithium monoxide is expected to be high due to its lack of electronic conductivity. A shift of the oxygen evolution onset potential to a more positive voltage was observed when the electrode was scanned down to 1.5 V which suggests the oxidation of additional Li_2O formed from the full reduction of Li_2O_2 to Li_2O. Figure 6C shows cyclability of the ORR/OER reactions in the potential range of 1.7 V to 3.7 V. In this case we have restricted the anodic potential in order to prevent the full recovery of the electrode surface after passivation with ORR products. The result is a gradual decrease in the activity of the electrode with accumulated products which passivate the microelectrode.

We have also studied ORR in $LiCF_3SO_3$/TEGDME electrolyte. Bell shaped voltammograms obtained in this electrolyte and the cyclic volatammograms obtained from cycling in the in the voltage range of 1.5 V to 4.5V are shown in Figure 7B. Unlike the behavior in $LiPF_6$/TEGDME electrolyte (Figure 7A), continuously collected current- potential profiles in $LiCF_3SO_3$/TEGDME does not show any decrease in current in all of the seven scans we examined.

It should be noted that, in contrast to the electrochemical responses in DMSO and DME-based electrolytes, Columbic efficiencies of the ORR in TEGDME was similar in both $LiPF_6$ and $LiCF_3SO_3$ electrolytes at 200 mV s^{-1}(Figure 8A). Continuous cycling of the potentials between 1.7 and 3.7 V in $LiCF_3SO_3$/TEGDME displayed cyclability performance (Figure 8B) similar to that observed in $LiPF_6$/TEGDME (Figure 6C). This observation was surprising due to the significantly different donor capabilities of the $CF_3SO_3^-$ (DN, 16.90) and PF_6^- (DN, 2.50) ions.[29] Apparently the solubility of the ORR products that are produced at potentials above 1.7 V is minimally influenced by the Li salt anion in TEGDME solutions. The major effect appears to come from TEGDME solvent itself probably through its solvation of Li^+ as discussed below from IR spectral data.

Lithium/O_2 cell performance with Li salt/TEGDME electrolytes.— We studied the effect of Li salt anions on ORR by examining the capacity of Li/O_2 cells fabricated with two electrolytes; i.e, 1M $LiCF_3SO_3$/TEGDME and 1M $LiPF_6$/TEGDME electrolytes. This study also looked at the effect of carbon cathode surface area on capacity by testing cells with cathodes prepared from both XC-72R carbon (with surface area of 233 m^2/gram) and EC300JD carbon (Ketjen Black with surface area of 802 m^2/gram), each with the two electrolytes. The Li/O_2 cells discharged at 0.1 mA cm^{-2} showed better discharge capacities with 1M $LiCF_3SO_3$/TEGDME than with 1M $LiPF_6$/TEGDME irrespective of the carbon cathode used in the cells (Figure 9).

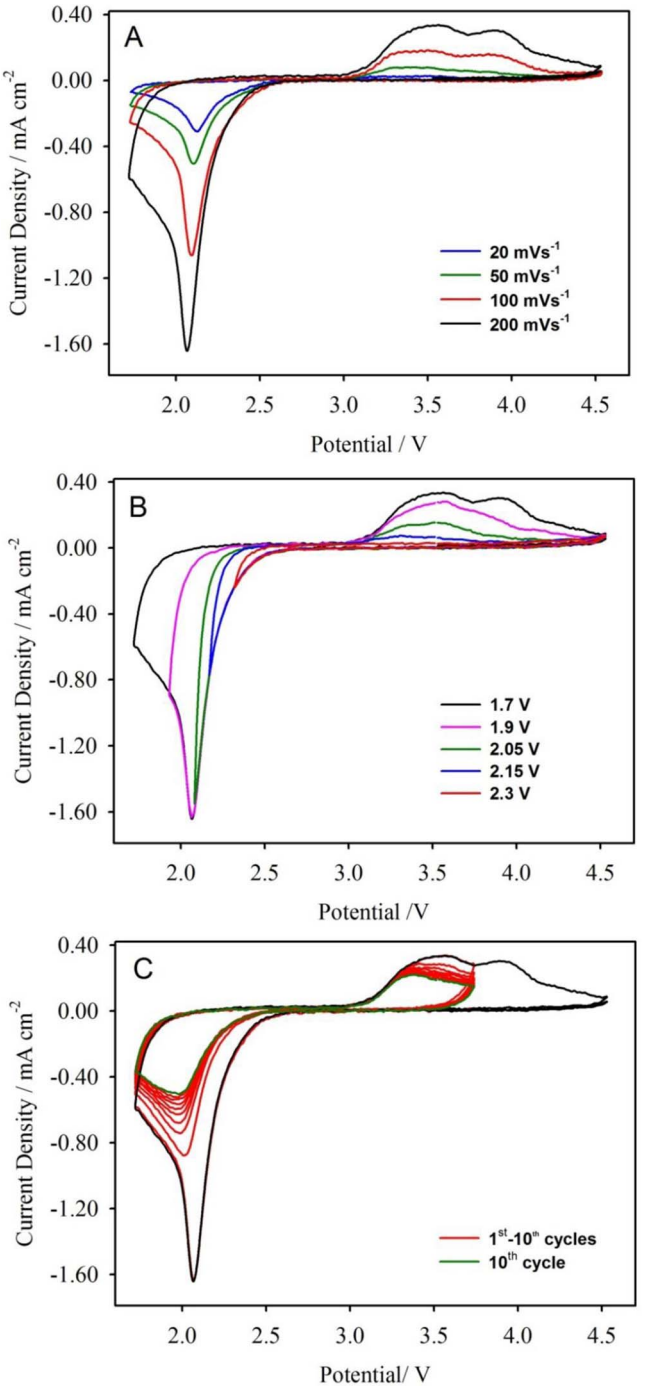

Figure 6. Cyclic voltammograms recorded at a 11 μm carbon disk in O_2 saturated $LiPF_6$/TEGDME. A) CVs collected at scan rates ranging from 20 mVs^{-1} to 200 mV s^{-1}, B) Anodic response at different cathodic limiting potentials, C) Cyclability of the ORR/OER in the potential range of 1.7 V and 3.6 V (initial scan at the full potential range from 1.7 V to 4.5 V is shown in black).

The discharge products accumulated in the cathodes of all four Li-O_2 cells were identified to be Li_2O_2 as evidenced by its characteristic X-ray diffraction pattern with d-values of 2.720, 2.568 and 1.565 Å.

Li/O_2 cells were cycled at a limited capacity of 400 $mAhg^{-1}$ with 1M $LiPF_6$/TEGDME and 1M $LiCF_3SO_3$/TEGDME electrolytes. The charge-discharge performances of the cells are shown in Figure 9C and 9D. The cell utilizing the $LiCF_3SO_3$/TEGDME electrolyte showed a slight advantage in cycle life although the advantage

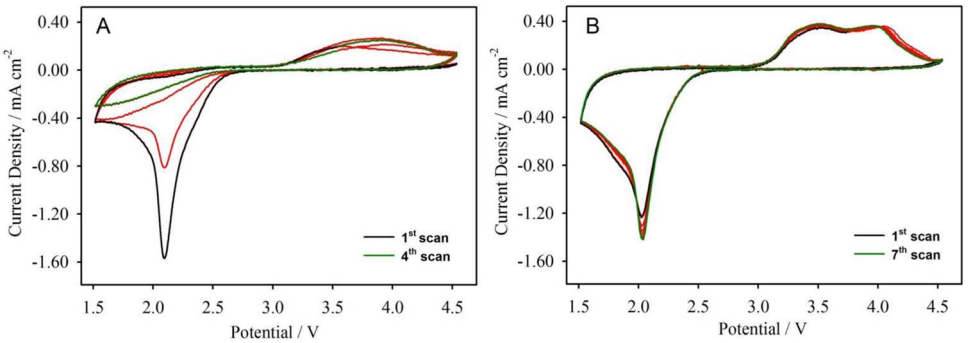

Figure 7. Cyclability of the oxygen reduction/evolution reaction in the potential range of 1.5 V and 4.5 V A) in 0.1 M $LiPF_6$/TEGDME, B) 0.1 M $LiCF_3SO_3$/TEGDME.

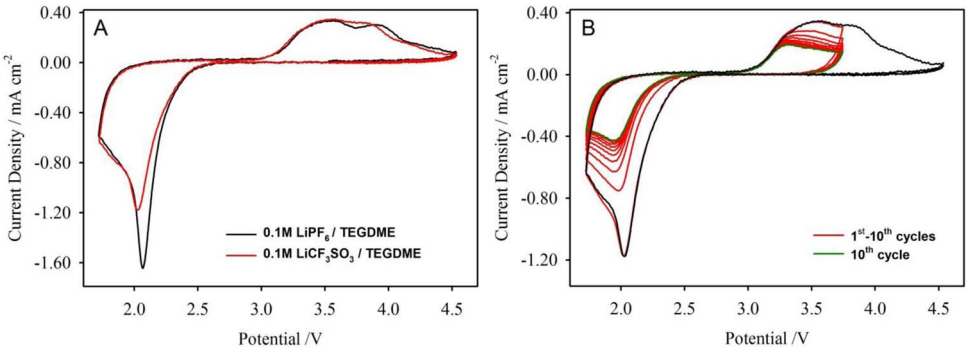

Figure 8. Cyclic voltammograms recorded at an 11 μm carbon microdisk at 200 mV s^{-1} in O_2 saturated A) 0.1M $LiPF_6$/TEGDME (black) and 0.1M $LiCF_3SO_3$/TEGDME (red). B) Cyclability of the ORR/OER in 0.1M $LiCF_3SO_3$/TEGDME in the voltage range of 1.7 V–3.7 V (black curve shows the initial scan in the voltage range of 1.5 V–4.6 V).

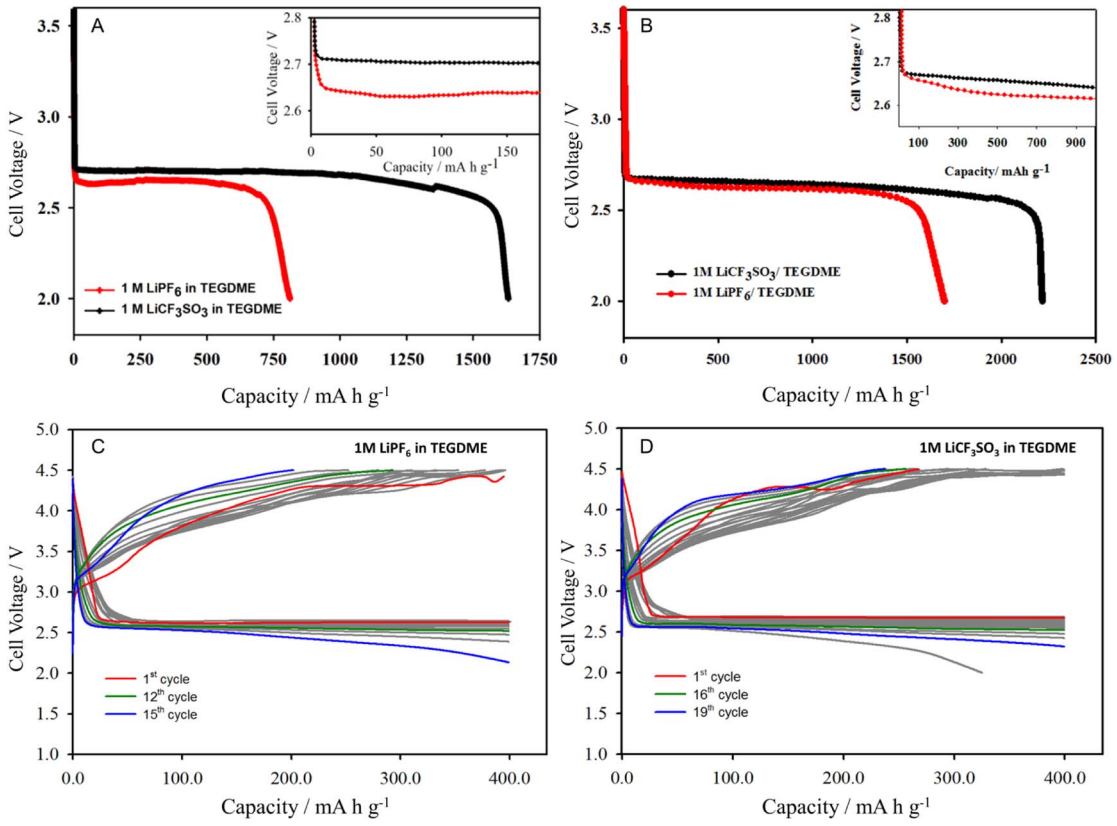

Figure 9. Galvanostatic discharge curves for Li/O_2 cells. A) XC72R carbon cathodes, B) Ketjenblack EC300JD carbon cathodes, both discharged at 0.1 mA cm^{-2} with $LiPF_6$/TEGDME and $LiCF_3SO_3$/TEGDME (insets shows the voltage scales expanded). Galvanostatic discharge-charge curves obtained for a Li/O_2 cell (KB300JD cathode) with C) $LiPF_6$/TEGDME, D) $LiCF_3SO_3$/TEGDME by limiting the capacity to 400 $mAhg^{-1}$ and limiting the charging potential to 4.5 V.

was not as significant as the capacity. We were unable to reproduce the superior results published by Scrosati et al. in a similar electrolyte using the super P carbon cathode.[30]

The low cycle life of the Li-O_2 cell is caused by many factors. First of all, the ORR products, superoxide and peroxide, react slowly with the solvents to degrade the electrolyte and to increase the cell's internal resistance from the accumulation of products from these reactions in the porous cathode. Another issue is the poor cycling efficiency of the Li anode due to reactions of the plated Li with the electrolyte during charging. Further studies to determine the contributions of each of these factors on the cycle life of the Li-air battery have to be performed and appropriate solutions found for each.

Assessing the solubility of the ORR products using rotating ring disk voltammetry.—We made an attempt to determine the relative quantities of the insoluble products deposited on the electrode during ORR with the aid of rotating ring disk electrode (RRDE) voltammetry. Before the RRDE experiments, O_2 reduction reaction electrochemistry on a Au disk electrode was recorded in each electrolyte in order to locate the oxidation potentials of the lithium oxides formed when the electrode was scanned cathodically from open circuit to the cathodic limit. Potential limited cyclic voltammograms recorded in this way in all Li salt/TEGDME –based electrolytes showed the first cathodic peak around 2.29 V and the corresponding anodic peak at 3.53 V. Data in Figure 10A shows the cyclic voltammogram obtained in $LiPF_6$/TEGDME electrolyte. It indicates a potential difference of 1.24 V between the reduction peak at 2.29 V and the oxidation peak at 3.53 V which is significantly more than 59 mV. This suggests that the oxidation peak observed at 3.53V is probably not due to the oxidation of superoxide ions. This peak is probably coming from the oxidation of Li_2O_2.

In the second part of the RRDE experiment, ORR ring-disk voltammetry in each electrolyte was performed at a gold ring-glassy carbon disk electrode in which the Au ring electrode was held at 3.53 V based on the above observation. Note that at 3.53 V both lithium superoxide and lithium peroxide should be oxidized. The RRDE voltammograms recorded at 800 rpm at 40 mV s^{-1} for O_2 reduction, in the two TEGDME electrolytes are shown in Figure 10B and 10C. The onset of the ORR at the carbon disk in 0.1M $LiPF_6$/TEGDME electrolyte occurred around 2.75 V. The ORR current quickly reached its peak current (-5×10^{-2} mA) at about 1.9 V and started to decrease. The oxidation reaction at the Au ring started when the carbon disk potential was around 2.25 V.

The ORR in $LiCF_3SO_3$/TEGDME electrolyte started at 2.75 V and the current magnitude continuously increased up to -3.5×10^{-2} mA remaining steady above 1.5 V. The oxidation reaction at the Au ring in this electrolyte started when the carbon disk was around 2.5 V. In $LiCF_3SO_3$/TEGDME, the ring current starts soon after the commencement of the ORR at the carbon disk. In other words superoxide formation at the carbon disk coincides with the emergence of the oxidation current at the Au ring. This indicates that a significant amount of superoxide ions are contributing to the oxidation current at the Au ring in $LiCF_3SO_3$/TEGDME. On the other hand, the oxidation current at the Au ring lags the ORR current at the carbon disk in $LiPF_6$/TEGDME electrolyte.

This information provides an insight on the stability of the superoxide ions in the two different electrolytes. The superoxide ions in the $LiCF_3SO_3$ -based electrolyte appear to have longer lifetimes and are readily transferred to the Au ring where they are oxidized. On the other hand, the superoxide ions in the $LiPF_6$ -based electrolyte appear to be less stable and are quickly decomposed to peroxide ions at the disk before being transferred to the ring where they are oxidized. The peroxide ions not only requires a larger oxidation over-potential, but also has a lower diffusion coefficient than the superoxide ions, both of which are contributing to the observed trend in ring current in PF_6^- -based electrolyte.

Oxygen electrochemistry in other Li salt/TEGDME electrolytes.—Oxygen electrochemistry was also recorded in two other Li-containing electrolytes namely, $LiClO_4$ and $LiN(SO_2CF_3)_2$ (LiTFSI).[31] Similar

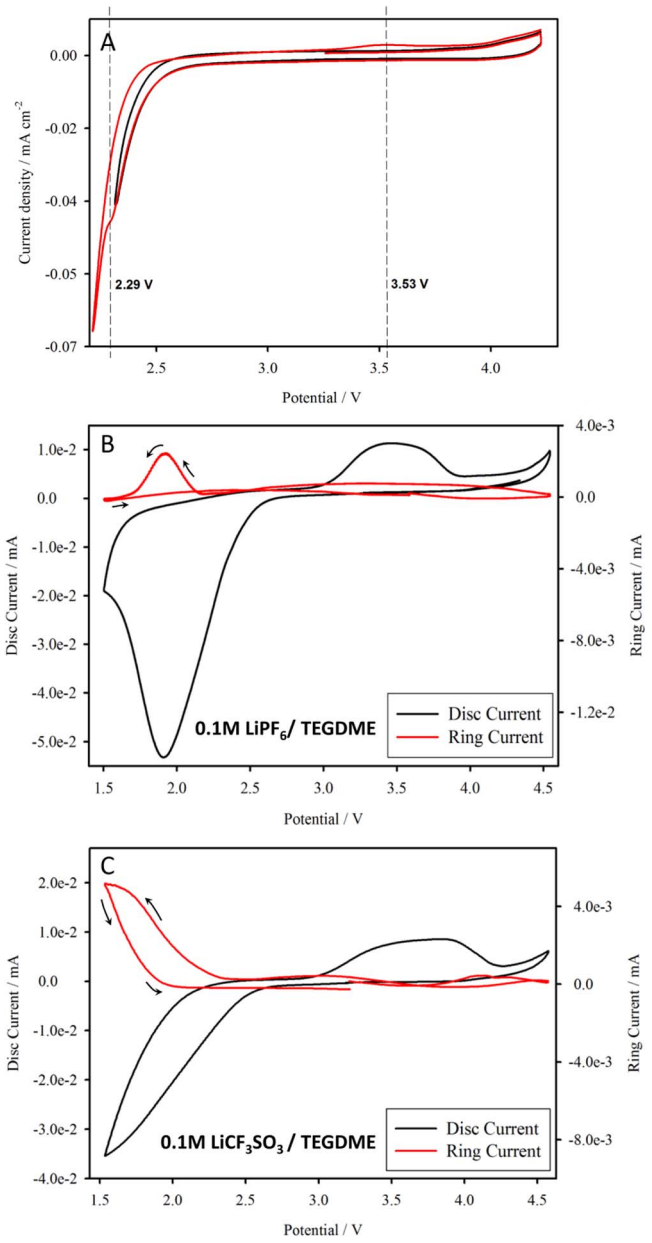

Figure 10. A) Cyclic voltammograms recorded in O_2 saturated $LiPF_6$/TEGDME at the Au macro disk. Rotating ring disk electrode response obtained in O_2 purged solutions (at 800 rpm at 40 mV s^{-1}) **B)** 0.1M $LiPF_6$/TEGDME and C) 0.1M $LiCF_3SO_3$/TEGDME (Disk response is shown in black and the ring response is shown in red).

bell shaped electrochemistry was observed in both these electrolytes suggesting the same overall ORR processes as we discussed above. Rotating ring disk response obtained suggested that electrochemistry in both $LiClO_4$ and $LiN(CF_3SO_2)_2$/TEGDME are similar to that observed in the $LiPF_6$/TEGDME system. It appears that even though sulfonyl oxygen atoms are present in the $N(CF_3SO_2)_2^-$ (TFSI) anion, the electron density is delocalized throughout this anion providing it with low donor properties than that in the $CF_3SO_3^-$ anion. As a result $LiN(CF_3SO_2)_2$ behaves more like $LiPF_6$.

The impact of the structure-property characteristics of $CF_3SO_3^-$ on ORR in ether electrolytes.— The preceding data suggest that the higher capacity of the Li/O_2 cell containing $LiCF_3SO_3$/TEGDME electrolyte is related to the structure of the electrolyte. This is reasonable considering that the initial ORR product superoxide (O_2^-) does not undergo chemical decomposition to insoluble Li_2O_2 right away

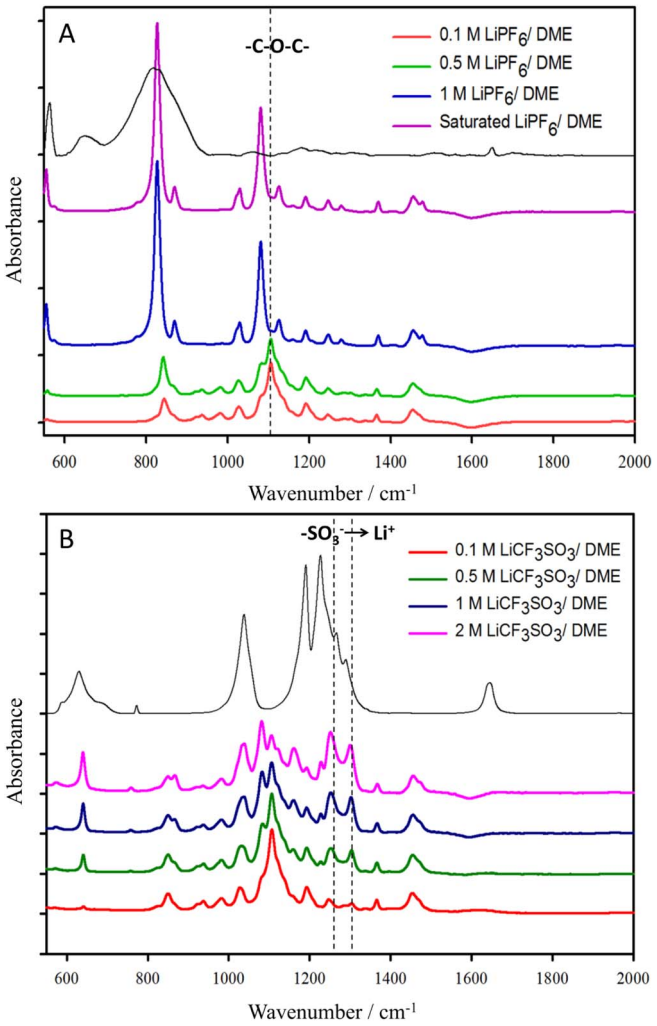

Figure 11. FT-IR spectra for Li salt solutions in DME for various salt concentrations. A) $LiPF_6$/DME (peak position of the solvent C-O-C vibration is shown by a dotted line at 1120 cm^{-1}), B) $LiCF_3SO_3$/DME (peak position of the asymmetric stretching vibrations of the ion paired sulfonyl groups are shown by dotted lines at 1260 and 1300 cm^{-1}). 'The top spectrum in black in (A) is **$LiPF_6$** and in (B) is **$LiCF_3SO_3$**.

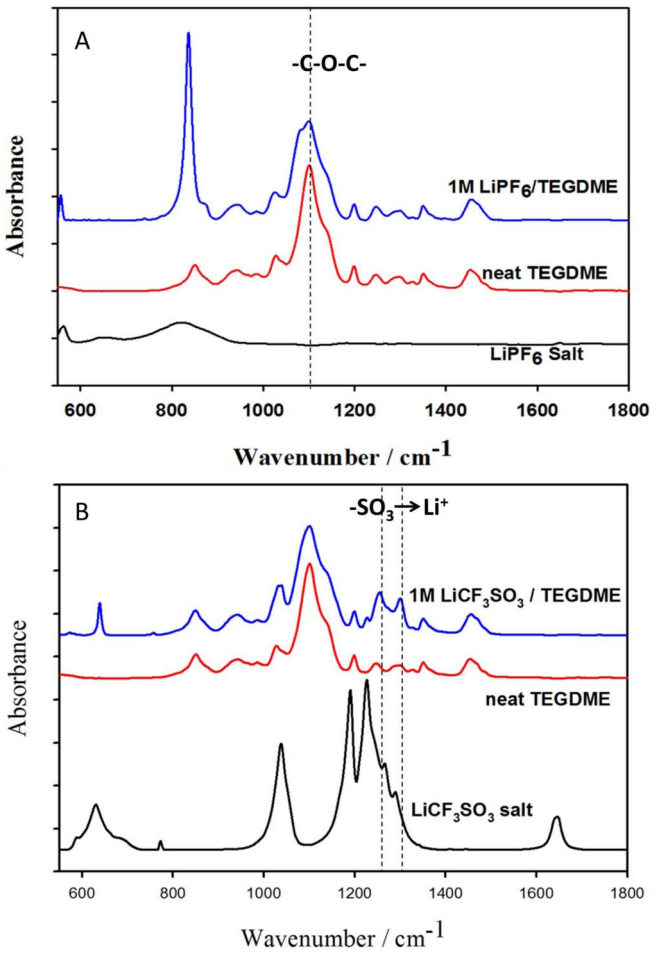

Figure 12. FT-IR spectra for Li salt solutions in TEGDME for various salt concentrations: A) $LiPF_6$/TEGDME (peak position of the solvent C-O-C vibration is shown by a dotted line at 1120 cm^{-1}), B) $LiCF_3SO_3$/TEGDME (peak position of the asymmetric stretching vibrations of the ion paired sulfonyl groups are shown by dotted lines at 1260 and 1300 cm^{-1}).

in this electrolyte. The superoxide, stabilized by this electrolyte, is apparently more soluble (as evidenced by the RRDE results) and is swiftly removed from the microelectrode surface by diffusion. The removal of the soluble superoxide from the carbon electrode surface to the $LiCF_3SO_3$/TEGDME electrolyte bulk in the porous electrode maintains the electrode surface less passivated and, as a result the electrode has higher activity to yield higher capacity in Li/O_2 cells. In order to characterize the structure of the electrolytes, the FT-IR spectra of Li salt solutions in DME and TEGDME were recorded and the data discussed below support this conclusion.

FT-IR spectral characterization of electrolyte structures.—FT-IR spectra of 1M $LiPF_6$ and 1M $LiCF_3SO_3$ in DME and TEGDME recorded from 550 cm^{-1} to 2000 cm^{-1} are shown in Figure 11. The vibrational absorption peak for the PF_6^- ion is observed at around 840 cm^{-1}. The symmetric stretching peak of the ether oxygen (C-O-C) linkage appears at about 1120 cm^{-1}. As more $LiPF_6$ is added to the $LiPF_6$/DME a shoulder peak appears at a lower frequency of 1090 cm^{-1}. With increasing concentration of $LiPF_6$ in DME, the peak at 1120 cm^{-1} completely disappears and when the $LiPF_6$ concentration is 1M (Figure 11A) the shoulder at 1090 cm^{-1} becomes the only absorption peak due to C-O-C stretching. A similar trend in the C-O-C absorption peak position is observed in $LiPF_6$/TEGDME also, Figure 12A.

The co-ordination (solvation) of Li^+ by the C-O-C linkage satisfactorily explains these spectral changes. When a significant amount of the $LiPF_6$ is added to DME or TEGDME, the C-O bonds become highly co-ordinated to Li^+ shifting the C-O-C absorption peak from 1120 cm^{-1} to the lower 1090 cm^{-1} at high $LiPF_6$ concentrations.

On the other hand, in $LiCF_3SO_3$/DME solution, the C-O-C absorption peak at 1120 cm^{-1} is still observed even at high Li^+ concentrations, Figure 11B. Both the 1120 cm^{-1} and 1090 cm^{-1} peaks are clearly visible in the spectra obtained for solutions of 1M $LiCF_3SO_3$/DME. This shoulder peak at 1090 cm^{-1} is not observed in the 1M $LiCF_3SO_3$/TEGDME solution.

This suggests that almost all of the DME molecules in the concentrated $LiPF_6$ solution (1M and up to saturated) are solvated by the Li^+ to form the solvent separated ion pair $Li^+(DME)_nPF_6^-$. A new peak which appears at 1130 cm^{-1} in these solutions is probably from the $-CH_3$ groups which are originally masked by the C-O peak. In the $LiCF_3SO_3$/DME electrolyte, it appeared that only a portion of the DME molecules solvate the Li^+. This is probably because, in the presence of $CF_3SO_3^-$ anion some of the ether oxygens of DME in the Li^+ co-ordination sphere are replaced by the sulfonyl oxygen of the triflate ions ($CF_3SO_3^-$). This is evident from the new strong peaks appearing between 1260 and 1300 cm^{-1} in this solution. The asymmetric stretching frequency of the free triflate ion appears at 1270 cm^{-1}. This peak degenerates to two peaks centering at 1270 cm^{-1} (i.e., at 1260 and 1300 cm^{-1}) when the sulfonyl oxygen is co-ordinated to Li^+. The substitution of some of the DME solvent in Li^+

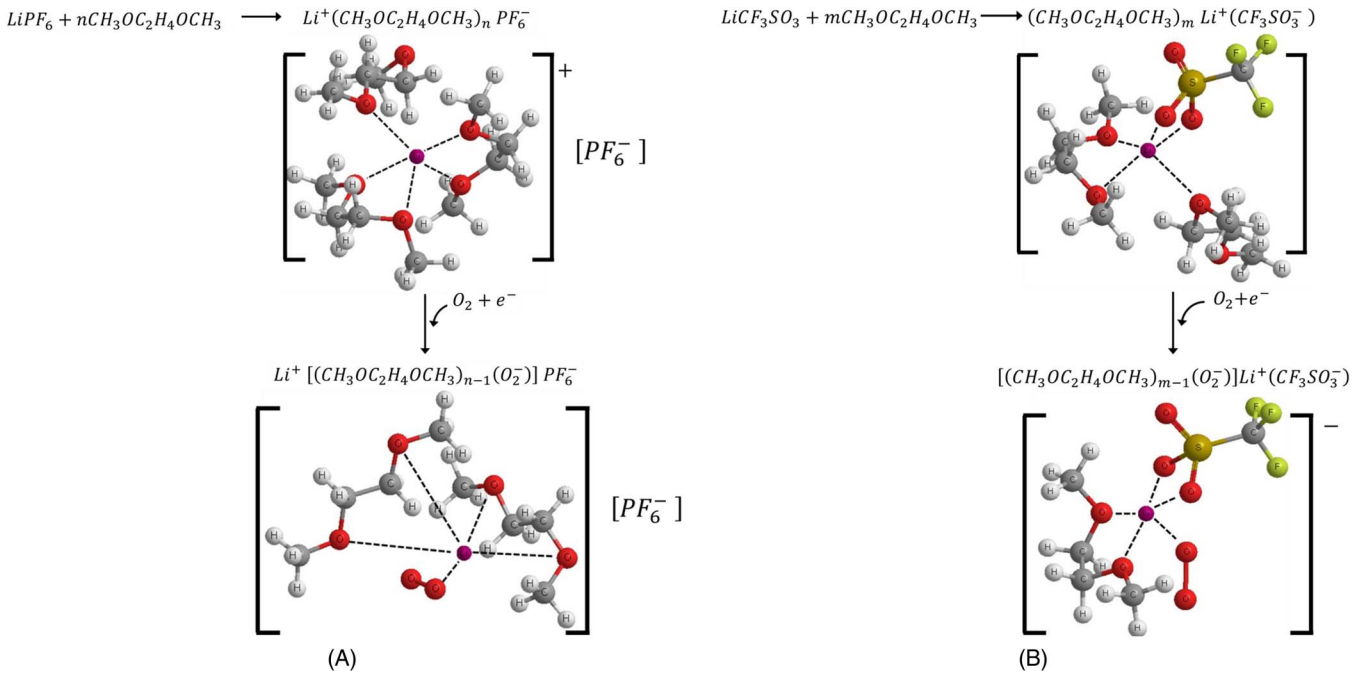

Scheme 1. A. Li^+ solvation and ion pair formation in $LiPF_6$/DME. B. Li^+ solvation and ion pair formation in $LiCF_3SO_3$/DME.

solvate by the $CF_3SO_3^-$ anion is understood when it is considered that the donor number of triflate (DN = 16.9) is closer to that of DME (DN = 20). In other words in the $LiCF_3SO_3$/DME electrolyte contact ion pairs of the type, $(DME)_mLi^+(CF_3SO_3)$ are formed.

A similar absorption spectral behavior is also observed in the spectra for the $LiCF_3SO_3$/TEGDME solutions in the range of 1200–1400 cm^{-1}, indicating sulfonyl oxygen coordination to Li^+ ions, Figure 12B.

It is reasonable to state from the FT-IR spectra detailed above that the electron donor capability and the conformational structure of the solvent molecule play a role on the ORR electrochemistry in Li/O_2 batteries. The PF_6^- has a very low electron donor capability (DN = 2.5) compared to $CF_3SO_3^-$ (DN = 16.9). Therefore, PF_6^- most probably does not form contact ion pairs with Li^+ in its DME solution (Scheme 1A). The Li^+ ions in this solution are coordinated to the solvent molecules to form the solvent separated ion pairs $Li^+(DME)_nPF_6^-$ between the Li^+ and the PF_6^- anion. The DME molecules in the Li^+ solvation sphere of $Li^+(DME)_nPF_6^-$ appear to rapidly exchange with the free DME present in the solution as evidenced by the presence of only one strong C-O-C IR absorption peak at 1090 cm^{-1} for the 1M solution although the Li^+ to DME concentration ratio is close to 1:8. It is also conceivable that once the superoxide ions are formed by the ORR, they will replace one of the ether oxygen in the solvation sphere around Li^+ in $Li^+(DME)_nPF_6^-$ to form the superoxide-containing ion pair $(Li^+[(DME)_{n-1}(O_2^-)]PF_6^-$ which can be seen as a contact ion pair between Li^+ and O_2^-. In short, the fluxional behavior of the DME in the coordination complex $Li^+(DME)_nPF_6$ makes the solvated Li^+ ions to be more accessible to superoxide ions in the DME/$LiPF_6$ solution and the contact ion-paired superoxide can readily abstract another Li^+ to be converted to Li_2O_2.

A different scenario seems to exist in the $LiCF_3SO_3$/DME electrolyte. The similar DN of DME and $CF_3SO_3^-$enables the latter to displace some of the DME molecules in the solvate and form contact ion pairs of the type $(DME)_mLi^+(CF_3SO_3^-)$. The anion can alter the conformation of the complex and position itself to form a bidentate coordination complex (solvate) with Li^+ since the electron density at the sulfonyl oxygen atoms is much higher than that at the ethereal oxygens. A bidentate coordination would provide strong $CF_3SO_3^-$ interactions with Li^+. The resulting solvated Li^+ cations are probably softer acids than in the corresponding $LiPF_6$ solution with the propensity to stabilize the O_2^- formed from ORR in the complex $[(DME)_{m-1}(O_2^-)]Li^+(CF_3SO_3^-)$, and to dissolve and remove the superoxide from the reaction site to maintain the carbon electrode more active for further reduction of O_2. This is probably the reason behind the significant improvement of the ORR electrochemistry in the presence of $CF_3SO_3^-$ in DME-based electrolytes.

The ORR observed in TEGDME can also be rationalized on similar structure-property characteristics of the solvates of Li^+ formed in these electrolytes.

Scheme 2A shows the tetraethylene glycol dimethyl ether (TEGDME) molecule (DN = 16.6) in its linear form. The FT-IR spectra of the 1M $LiPF_6$ solution in TEGDME indicate that only a fraction of the TEGDME is co-ordinated to the Li^+. This is consistent with TEGDME solvating the Li^+ cation by forming a caged structure around Li^+ (scheme 2B).[32] In this case the solvated TEGDME molecule in the $Li^+(TEGDME)PF_6^-$ complex is not easily exchanged with free TEGDME. This solvent separated ion pair solvate structure is apparently stable. The superoxide ion formed by the ORR, because of its basicity, is probably able to replace one of the ethereal oxygens in Li^+(TEGDME) to form a superoxide-containing ion pair of the structure, $Li^+[(TEGDME)(O_2^-)]PF_6^-$. The superoxide ion becomes somewhat shielded inside the caged Li^+(TEGDME) complex. In this structure, O_2^- probably cannot easily access other solvated Li^+ ions and the result is longer lifetime and solubility for the superoxide.

Scheme 2C shows the probable ORR sequence in the presence of $CF_3SO_3^-$ anions. The very similar DN of TEGDME and $CF_3SO_3^-$ implies that the triflate could enter into the co-ordination sphere with TEGDME by substituting for some of the Li^+–O-bonds in the Li^+(TEGDME) solvate with Li^+–O=S bonds to form a contact ion pair of the type (TEGDME)$Li^+(CF_3SO_3^-)$. Even though the caged solvate structure is somewhat altered in this case, the stability imposed by the strong interaction between the sulfonyl oxygens with the Li^+ ions will restore or even enhance the stability of the $Li^+[(TEGDME)(O_2^-)](CF_3SO_3^-)$ complex formed with superoxide. The higher capacity obtained in Li/O_2 cells utilizing $LiCF_3SO_3$/TEGDME electrolyte is consistent with the stability of the superoxide ions shown in scheme 2C, its increased solubility and diffusion away from the carbon electrode surface to the electrolyte bulk in the pores of the electrode where it decomposes to Li_2O_2.

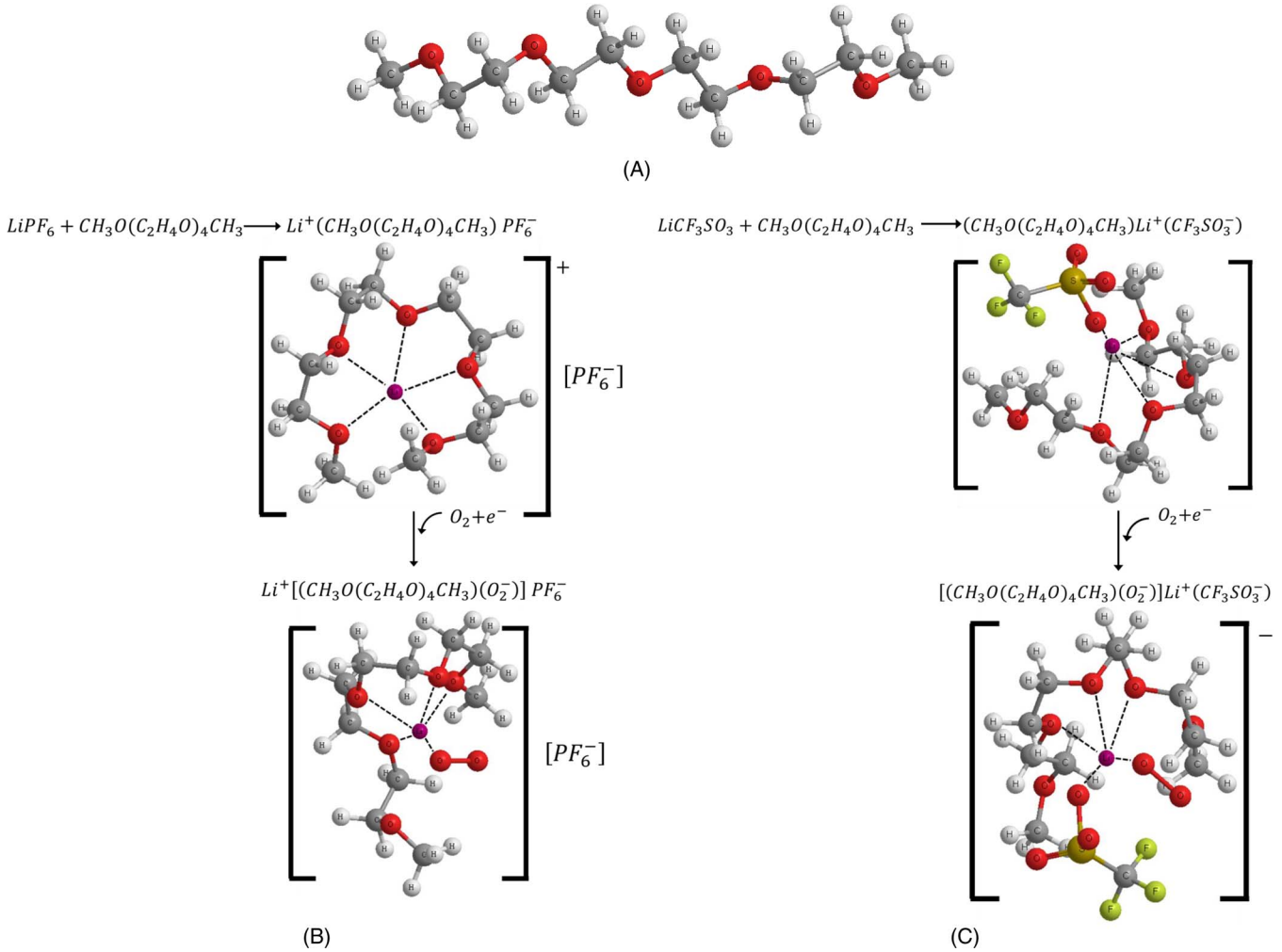

Scheme 2. A. Linear Structure of TEGDME. B. Li^+ solvation and ion pair formation in $LiPF_6$/TEGDME. C. Li^+ solvation and ion pair formation in $LiCF_3SO_3$/TEGDME.

Solvation enthalpy vs. lattice enthalpy.—In general a crystalline solid like Li_2O_2 dissolves in a solvent when its solvation energy with the solvent exceeds its lattice energy. The following calculations indicate that Li_2O_2 will not be soluble in TEGDME or DME but LiO_2 could. The Enthalpy of solvation calculated for Li^+ in diethyl ether to form Li^+(diethyl ether)$_5$ using Drago's equation[33] we described previously is about 209 kcal/mole. On the other hand, the lattice energy calculated for Li_2O_2 is 619.4 kcal/mole.[34] It is unlikely that the lithium peroxide dissolves in any of these ether based electrolytes. Lattice energy for LiO_2 has been calculated to be 210 kcal/mole.[35] This value is comparable to the above mentioned estimated solvation energy of Li^+ in ether-based electrolytes. The enthalpy data provide a rational explanation for the solubility of lithium superoxide complexes discussed above in the ether electrolytes. The stable complexes are able to dissolve in the ether electrolytes, move away from the electrode surface to the electrolyte in the electrode pores and decompose there eventually to form Li_2O_2. In this way the porous electrode performs better in the $LiCF_3SO_3$-based electrolytes in which the suproxide complexes are more stable and soluble to yield higher capacities in the Li/O_2 cells.

Conclusions

We have shown that the conducting salt anion does not affect oxygen transport in TBA salt-based electrolytes in 1,2-dimethoxyethane. As a result we have been able to determine O_2 solubility and diffusion coefficients in these electrolytes. We have also found higher oxygen transport parameters in electrolytes prepared from both the low viscosity DME and high viscosity TEGDME compared to that in DMSO. We attribute this to the electrolyte structures.

We have found that the discharge capacities of Li/O_2 cells utilizing $LiCF_3SO_3$ /TEGDME solutions are higher than in those containing $LiPF_6$/TEGDME. Our microelectrode and RRDE data combined with IR spectra suggest that the higher capacity in $LiCF_3SO_3$-based Li/O_2 cells is due to the increased stability and solubility of the ion pair specie formed in the electrolyte between the initial ORR product superoxide (O_2^-) and the solvated Li^+ with a structure such as [(TEGDME)(O_2^-)]Li^+($CF_3SO_3^-$) in which the Li^+ resides in a TEGDME cage. The PF_6^- anion does not form a similar contact ion pair with Li^+ in DME or TEGDME because of the very low DN of PF_6^- compared to that of the TEGDME solvent and the $CF_3SO_3^-$ anion. This study further affirms the electrolyte-controlled ORR processes in non-aqueous Li/O_2 batteries.

Acknowledgments

We sincerely thank U.S. Army CERDEC for the financial support provided through subcontract No. GTS-S-13-025 for this work.

References

1. K. M. Abraham, P. G. Bruce, and L. J. Hardwick, *MRS Bull*, **36**, 506 (2011).
2. C. O. Laoire, S. Mukerjee, K. M. Abraham, E. J. Plichta, and M. A. Hendrickson, *The Journal of Physical Chemistry C*, **114**, 9178 (2010).

3. M. J. Trahan, S. Mukerjee, E. J. Plichta, M. A. Hendrickson, and K. M. Abraham, *Journal of The Electrochemical Society*, **160**, A259 (2013).
4. C. J. Allen, J. Hwang, R. Kautz, S. Mukerjee, E. J. Plichta, M. A. Hendrickson, and K. M. Abraham, *The Journal of Physical Chemistry C*, **116**, 20755 (2012).
5. C. J. Allen, S. Mukerjee, E. J. Plichta, M. A. Hendrickson, and K. M. Abraham, *The Journal of Physical Chemistry Letters*, **2**, 2420 (2011).
6. C. O. Laoire, S. Mukerjee, K. M. Abraham, E. J. Plichta, and M. A. Hendrickson, *The Journal of Physical Chemistry C*, **113**, 20127 (2009).
7. C. O. Laoire, S. Mukerjee, K. M. Abraham, E. J. Plichta, and M. A. Hendrickson, *The Journal of Physical Chemistry C*, **114**, 9178 (2010).
8. I. Gunasekara, S. Mukerjee, E. J. Plichta, M. A. Hendrickson, and K. M. Abraham, *Journal of The Electrochemical Society*, **161**, A381 (2014).
9. I. Gunasekara, S. Mukerjee, and K. M. Abraham, Microelectrode Investigations of Oxygen Reduction Reactions in Lithium-Air Batteries, *ECS Meeting Abstracts*, **MA2013-02**, 449 (2013).
10. M. J. Trahan, I. Gunasekara, S. Mukerjee, E. J. Plichta, M. A. Hendrickson, and K. M. Abraham, *Journal of The Electrochemical Society*, **161**, A1706 (2014).
11. K. M. Abraham, *Journal of The Electrochemical Society*, **162**, A3021 (2015).
12. B. D. McCloskey, D. S. Bethune, R. M. Shelby, G. Girishkumar, and A. C. Luntz, *The Journal of Physical Chemistry Letters*, **2**, 1161 (2011).
13. W. Xu, K. Xu, V. V. Viswanathan, S. A. Towne, J. S. Hardy, J. Xiao, Z. Nie, D. Hu, D. Wang, and J.-G. Zhang, *Journal of Power Sources*, **196**, 9631 (2011).
14. V. S. Bryantsev, V. Giordani, W. Walker, M. Blanco, S. Zecevic, K. Sasaki, J. Uddin, D. Addison, and G. V. Chase, *The Journal of Physical Chemistry A*, **115**, 12399 (2011).
15. D. Aurbach, M. Daroux, P. Faguy, and E. Yeager, *Journal of Electroanalytical Chemistry and Interfacial Electrochemistry*, **297**, 225 (1991).
16. M. A. Rivas, T. P. Iglesias, S. M. Pereira, and N. Banerji, *The Journal of Chemical Thermodynamics*, **38**, 245 (2006).
17. C. F. Riadigos, R. Iglesias, M. A. Rivas, and T. P. Iglesias, *The Journal of Chemical Thermodynamics*, **43**, 275 (2011).
18. K. M. Abraham, Z. Jiang, and B. Carroll, *Chemistry of Materials*, **9**, 1978 (1997).
19. A. J. Wain, G. G. Wildgoose, C. G. R. Heald, L. Jiang, T. G. J. Jones, and R. G. Compton, *The Journal of Physical Chemistry B*, **109**, 3971 (2005).
20. C. P. Winlove, K. H. Parker, and R. K. C. Oxenham, *Journal of Electroanalytical Chemistry and Interfacial Electrochemistry*, **170**, 293 (1984).
21. I. Gunasekara, M. Lee, D. Abbott, and S. Mukerjee, *ECS Electrochemistry Letters*, **1**, F16 (2012).
22. C. Laoire, S. Mukerjee, E. J. Plichta, M. A. Hendrickson, and K. M. Abraham, *Journal of The Electrochemical Society*, **158**, A302 (2011).
23. M. J. Trahan, Q. Jia, S. Mukerjee, E. J. Plichta, M. A. Hendrickson, and K. M. Abraham, *Journal of The Electrochemical Society*, **160**, A1577 (2013).
24. L. Cecchetto, M. Salomon, B. Scrosati, and F. Croce, *Journal of Power Sources*, **213**, 233 (2012).
25. Y.-C. Lu, H. A. Gasteiger, M. C. Parent, V. Chiloyan, and Y. Shao-Horn, *Electrochemical and Solid-State Letters*, **13**, A69 (2010).
26. Y.-C. Lu, H. A. Gasteiger, E. Crumlin, R. McGuire, and Y. Shao-Horn, *Journal of The Electrochemical Society*, **157**, A1016 (2010).
27. M. Salomon, *Journal of Power Sources*, **26**, 9 (1989).
28. J. Read, *Journal of The Electrochemical Society*, **153**, A96 (2006).
29. W. Linert, A. Camard, M. Armand, and C. Michot, *Coordination Chemistry Reviews*, **226**, 137 (2002).
30. H.-G. Jung, J. Hassoun, J.-B. Park, Y.-K. Sun, and B. Scrosati, *Nature Chemistry*, **4**, 579 (2012).
31. E. Nasybulin, W. Xu, M. H. Engelhard, Z. Nie, S. D. Burton, L. Cosimbescu, M. E. Gross, and J.-G. Zhang, *The Journal of Physical Chemistry C*, **117**, 2635 (2013).
32. U. Olsher, R. M. Izatt, J. S. Bradshaw, and N. K. Dalley, *Chemical Reviews*, **91**, 137 (1991).
33. R. S. Drago, D. C. Ferris, and N. Wong, *Journal of the American Chemical Society*, **112**, 8953, (1990).
34. R. H. Wood and L. A. D'Orazio, *The Journal of Physical Chemistry*, **69**, 2558 (1965).
35. R. H. Snow, *Thermodynamic Evaluation of the Possibility of Lithium Superoxide Production Technical Report*, Aerospace Medical Research Laboratories, (1965).